Three-dimensional reconstruction and analysis of the tubular system of vertebrate skeletal muscle

Isuru D. Jayasinghe and Bradley S. Launikonis*

School of Biomedical Science, The University of Queensland, Brisbane, QLD 4072, Australia

*Author for correspondence (b.launikonis@uq.edu.au)

Accepted 7 June 2013
Journal of Cell Science 126, 4048–4058

doi: 10.1242/jcs.131565

Summary

Skeletal muscle fibres are very large and elongated. In response to excitation there must be a rapid and uniform release of Ca^{2+} throughout for contraction. To ensure a uniform spread of excitation throughout the fibre to all the Ca^{2+} release sites, the muscle internalizes the plasma membrane, to form the tubular (t-) system. Hence the t-system forms a complex and dense network throughout the fibre that is responsible for excitation–contraction coupling and other signalling mechanisms. However, we currently do not have a very detailed view of this membrane network because of limitations in previously used imaging techniques to visualize it. In this study we serially imaged fluorescent dye trapped in the t-system of fibres from rat and toad muscle using the confocal microscope, and deconvolved and reconstructed these images to produce the first three-dimensional reconstructions of large volumes of the vertebrate t-system. These images showed complex arrangements of tubules that have not been described previously and also allowed the association of the t-system with cellular organelles to be visualized. There was a high density of tubules close to the nuclear envelope because of the close and parallel alignment of the long axes of the myofibrils and the nuclei. Furthermore local fluorescence intensity variations from sub-resolution tubules were converted to tubule diameters. Mean diameters of tubules were 85.9 ± 6.6 and 91.2 ± 8.2 nm, from rat and toad muscle under isotonic conditions, respectively. Under osmotic stress the distribution of tubular diameters shifted significantly in toad muscle only, with change specifically occurring in the transverse but not longitudinal tubules.

Key words: Tubular system, Transverse tubules, t-tubules, Reconstruction, Nucleus, Confocal

Introduction

The tubular (t-) system of skeletal muscle is an internalization of the plasma membrane and remains continuous with the extracellular space. This membrane system reaches the Ca^{2+} release sites on the repeating contractile unit of the fibre, the sarcomere. This arrangement effectively solves a surface area to volume problem for the fibre, allowing the fast and uniform propagation of excitation to these sites virtually simultaneously, reducing the delay to Ca^{2+} release activation to the briefest possible time (Melzer et al., 1995). There are several obstacles to the t-system forming the required network for this function. In the fibre there are densely packed myofibrils that are not always aligned. In addition there are membrane bound organelles that the t-system maintains a close spatial association with, such as the sarcoplasmic reticulum (SR) at each sarcomere, or otherwise navigate around, such as nuclei and mitochondria. The t-system must also maintain its integrity during contraction and stretching of the muscle so that muscle function is not compromised. Skeletal muscle has evolved a dense and highly structured t-system membrane network to achieve this.

The t-system network primarily consists of transverse tubules that extend transversely along the A–I boundary of the sarcomere in mammals (Eisenberg and Kuda, 1975; Eisenberg and Kuda, 1976; Franzini-Armstrong et al., 1988) or z-lines in other vertebrate muscle (Peachey, 1965; Eisenberg and Eisenberg, 1968; Franzini-Armstrong et al., 1975). Thus mammalian skeletal muscle t-system is distinguished from that of other vertebrates by having two compared to one transverse tubule per sarcomere. In each case the transverse tubule docks with the terminal cisternae of the SR at these sites on the sarcomere. Infrequently, transverse tubules are connected by longitudinal tubules and at junctions of misaligned myofibrils where the t-system realigns itself with tubules that in an array form helicoid structures (Peachey and Eisenberg, 1978; Launikonis and Stephenson, 2004; Edwards and Launikonis, 2008).

Because the t-system maintains an extracellular–intercellular interface throughout the fibre and the normal separation of charges, all tubule membranes are excitable. Action potentials can propagate solely within this network for long distances (Posterino et al., 2000; Edwards et al., 2012) while its lumen restricts the movement of solutes along the long axis of the fibre (Edwards and Launikonis, 2008). The latter property underscores the role of the t-system in compartmentalizing its luminal solutes that would otherwise affect its excitability. The t-system is also a dynamic structure, changing its volume or vacuolating with osmotic stress or other factors (Krolenko et al., 1995; Krolenko and Lucy, 2001; Launikonis and Stephenson, 2002a; Launikonis and Stephenson, 2004).

What we know of the t-system structure is mostly from imaging of fixed fibres by electron microscopy (EM) or lower resolution fluorescence imaging. A limitation of thin-section EM is shrinkage of fixed and dehydrated preparations, which underestimate spatial dimensions (Eisenberg et al., 1974) and exclude the possibility of observing dynamic changes in the t-system. Optical studies could measure fluorescent dyes in the extracellular space of isolated and functional muscle fibres.

These studies consistently calculated larger spatial dimensions of the t-system compared to EM studies (Endo, 1964; Soeller and Cannell, 1999; Launikonis and Stephenson, 2002b). Furthermore the advantage of imaging muscle cells with an applied extracellular dye was reconstructions of large volumes of the t-system were made possible because of the imaging range of fluorescence microscopes, as performed in cardiomyocyte (Soeller and Cannell, 1999). Large volume 3D reconstructions using fluorescence microscopy provides contrasting and complimentary information compared to the 3D reconstructions from EM, which are limited to working within much smaller volumes (Peachey and Eisenberg, 1978; Wagenknecht et al., 2002).

Fluorescence optical imaging of the skeletal muscle t-system has been performed using techniques of dye-trapping facilitated by mechanical skinning (Edwards et al., 2012). Trapping dye in the t-system of skinned fibres offers the advantage for optical microscopy of removing an otherwise thick layer of fluorescence from around the fibre, which bleeds into the optical layers of intact fibre preparations (Lamb et al., 1995; Launikonis and Stephenson, 2002a). However a problem that has not been addressed by optical imaging studies is the asymmetric blurring of the sub-resolution tubular structures and the challenge in calibrating intensity information from the local sub-resolution tubule volumes of such images (Soeller and Cannell, 1999). In the present study, we have combined fluorescent-dye trapping in the sealed t-system with image analysis protocols used previously (Soeller and Cannell, 1999) that we have improved upon here. Confocal imaging and image deconvolution of this study has produced the first 3D reconstructions of the t-system of functional skeletal muscle fibres. This technique also allows the t-system to be viewed with associated organelles on an appropriate scale while also allowing determination of local tubular spatial dimensions (to a detection threshold of 40 nm), which we found to vary along tubules and change with osmotic stress.

Results

Morphology of the mammalian tubular system

Trapping of membrane-impermeable fluorescent probes within the t-system by the means of mechanical skinning was used as the primary approach for imaging the t-system in skeletal muscle fibres. Fluo-5N was used as the preferred volumetric marker of the t-system because it is a small molecule that diffuses easily into all compartments of the t-system and the green emission (~530 nm) provides superior resolution in imaging compared to other probes with longer emission wavelengths. Z-stacks of longitudinal confocal sections of skinned fibres with 5 mM Fluo-5N salt trapped within the sealed t-system were obtained. Fig. 1A shows a single confocal section from a deconvolved image stack of an extensor digitorum longus (EDL) fibre from an adult rat. As expected, doublets of fine transverse tubules were observed in sarcomeric periodicity.

Fig. 1B illustrates a surface-rendered reconstruction of a 3D skeleton constructed from the Fluo-5N fluorescence in a 38×20×10 μm volume of the fibre shown in A. The periodic

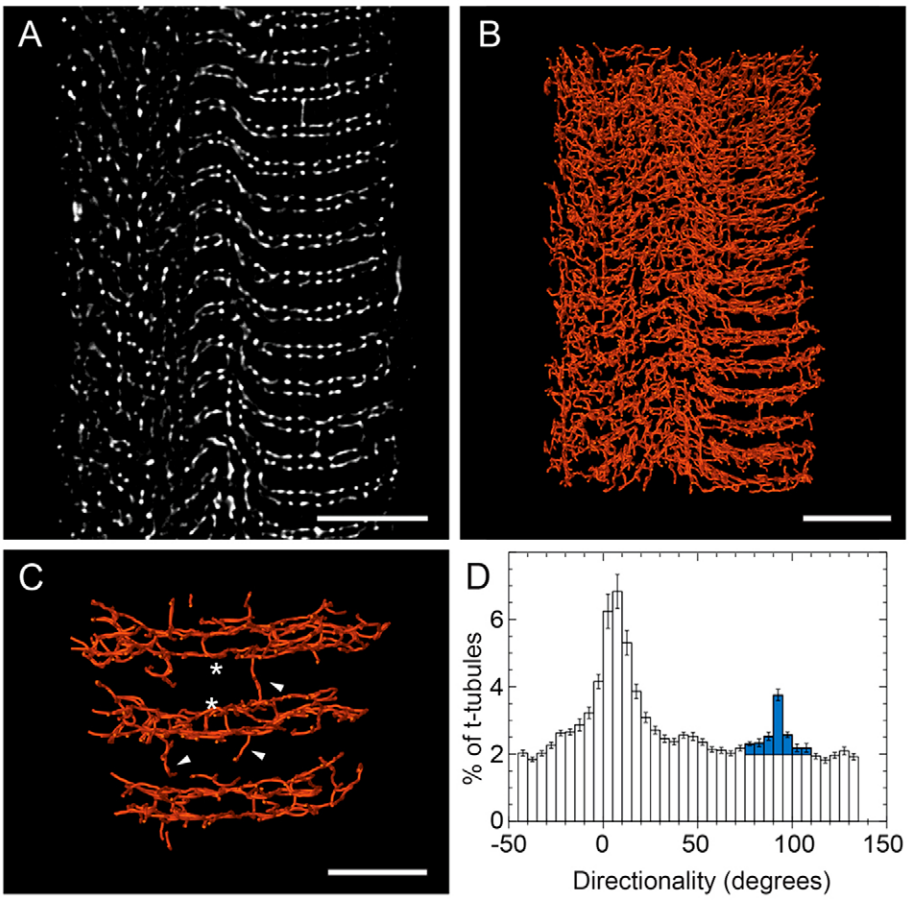

Fig. 1. Reconstruction of a 3D skeleton of the mammalian skeletal muscle t-system. (**A**) A single confocal section of a mechanically skinned adult rat EDL fibre with 5 mM Fluo-5N trapped within the t-system. Scale bar: 6 μm. (**B**) 3D surface rendered skeleton of the t-system reconstructed from a 38×20×10 μm deconvolved confocal image volume illustrates the connectivity of the mammalian t-system across the width of the fibre. Note that the rows of tubule doublets are clearer in some regions of the 3D skeleton than others because of angled alignment of sarcomeres across the width of the fibre. Scale bar: 5 μm. (**C**) The magnified view of a 6×8×10 μm sub-volume of the skeleton. Also indicated are the longitudinal tubules extending across the A-band (arrowheads) and I band (asterisks). Scale bar: 2 μm. (**D**) A histogram of the percentage of tubules as a function of the directional angle in relation to the transverse plane of the fibre indicates 4.9% of tubules extend longitudinally either across the A-band or the I-band.

morphology of tubule doublets flanking each z-line was apparent in the surface-rendered skeleton. However, the strength of the periodicity observed was highly dependent on the tilt angle of the volume, due to the non-planar configuration of z-lines (Peachey and Eisenberg, 1978). A notable subset of tubules appeared to extend in the longitudinal direction, further contributing to the dense mesh-like appearance of the t-system skeleton. Fig. 1C illustrates a higher magnification of a 6×8×10 µm sub-volume of the skeleton shown in B. This view of the t-system reveals a more complex geometry of the longitudinal tubules than previously reported. Tubules extending across the A-band (arrowheads) could join adjacent transverse tubules and others were blind-ended. Shorter longitudinal tubules extending across the I-band were also detected (asterisk). The directionality analysis of the skeletons is shown as a histogram of the percentage of tubular connections as a function of their angle relative to the transverse plane. In addition to the large primary peak at 0° relating to tubules extending transversely at the A–I boundaries, a secondary peak was observed at ~90°. 15.88±0.34% (mean ± s.e.m.) of the tubular connections extended between angles of 75° and 110° from the transverse plane of the fibre. This is illustrated by the shaded bars of the histogram of the percentage of tubules as a function of their relative directionality angle shown in Fig. 1D. Analysis of manually selected regions exclusively consisting of transverse tubules reported no secondary peak at ~90°, although a uniform tubule distribution between 75° and 110° accounted for ~10.98% of all tubules in these regions. The fraction of tubules extending in the longitudinal direction can be corrected by subtracting this uniformly distributed baseline from the overall distribution of tubule directionality between the angles of 75° and 110° (supplementary material Fig. S2). Therefore, the corrected percentage of tubules identified as 'longitudinal' was ~4.9%.

Morphology of the amphibian tubular system

The same approach was used for imaging and reconstructing the tubular system of toad iliofibularis fibres. Fig. 2A is a single confocal image from a z-series of confocal images of a mechanically skinned fibre from toad with 5 mM Fluo-5N trapped within the t-system. In contrast to the t-system in rat EDL muscle, the toad t-system consisted of a single row of tubules extending transversely at each z-line, as expected (Eisenberg and Eisenberg, 1968). Similar to the rat t-system, tubules extending longitudinally were observed. Most longitudinal tubules spanned the entire length of the sarcomere to connect with flanking transverse tubules while notably some were much shorter and blind-ended (arrowheads). A distinct feature of the toad t-system was regions within the fibres containing high densities of longitudinal tubules that extended across several sarcomeres bridging many transverse tubules at consecutive z-lines. These 'bundles' of longitudinal tubules were typically observed for lengths of 10–30 sarcomeres and were not exclusive to regions of sarcomere misregistration [which usually gives rise to oblique branching of the transverse tubules (Launikonis and Stephenson, 2004)]. An example is indicated by asterisks in a surface-rendered 3D skeleton of a 34×26×7 µm region in a toad fibre (Fig. 2B). The magnified view of the skeleton (Fig. 2C) shows that longitudinal tubules in these fibres may have complex tortuosity or angles. The histogram of the percentage of tubules plotted as a function of the directional angle relative to the transverse plane (Fig. 2D) shows a large primary peak near 0°

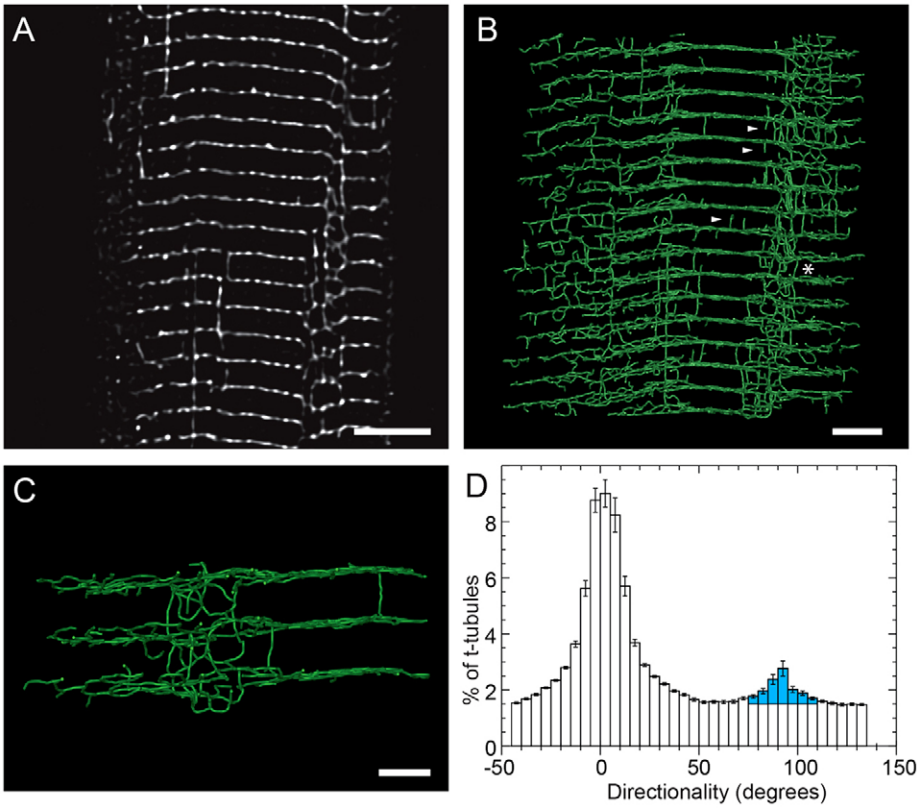

Fig. 2. Reconstruction of a 3D skeleton of the amphibian skeletal t-system. (**A**) A single confocal section of a mechanically skinned toad iliofibularis fibre with 10 mM Fluo-5N trapped within the t-system. Scale bar: 5 µm. (**B**) A 3D surface rendered skeleton of the toad t-system reconstructed from a 34×26×7 µm deconvolved confocal image volume illustrating the 3D geometry of tubules. Regions containing a high density of longitudinal tubules (asterisk) were observed. Some of the longitudinal tubules (arrowheads) also appeared to be blind-ended at one end. Scale bar: 4 µm. (**C**) The magnified view of a 9×5×6 µm sub-volume of the 3D skeleton further illustrates the geometries of the longitudinal tubules and transverse tubules seen at the z-lines. Scale bar: 2 µm. (**D**) Directionality analysis illustrated by a histogram of the percentage of tubules as a function of the angle relative to the transverse plane shows that a minimum of 2.2% of tubules of the t-system were longitudinal tubules.

and a smaller secondary peak at 90°. The secondary peak appeared broader than that observed in the same analysis in rat fibres (Fig. 1D). It comprises 12.68±0.27% of tubules between the angles of 75° and 110° (shaded bars). Analysis of regions devoid of longitudinal connections still detected ~10.5% of all tubular connections between these angles. Therefore, the corrected percentage of tubules identified as 'longitudinal' was ~2.2%.

Spatial association between the t-system and the nucleus

Nuclei of mechanically skinned fibres were stained with propidium iodide (PI) in order to visualize the tubular geometries in reference to nuclei. Fig. 3A shows the lateral view of the surface of a rat fibre. The peripherally located nuclei (surface rendered in transparent blue) appear to be exposed on its lateral surface in the mechanically skinned fibre while the dense tubular network (skeleton shown in orange) extends around and medially to the nuclei. The tubules observed near the surface of the fibre appeared to be denser and less organized into transverse rows, bearing the structural hallmarks of the sub-sarcolemmal tubular network (SSTN) (Jayasinghe et al., 2013). However, in the lateral view of the 10 µm deep volume it was also possible to view the double rows of transverse tubules (arrowheads). The x–z view of the same volume across a 5 µm deep slice is shown in Fig. 3B. The peripherally located nuclei appeared to be partially chaliced by the t-system around its medial side. Overlapping loops observed in the t-system skeleton in regions around the nucleus illustrate t-tubules wrapping around the myofibrils running orthogonally to the image plane.

In longitudinal view of nuclei in toad fibres (Fig. 3C), a dense mesh of tubules appears to closely wrap around the centrally located nuclei. The nuclear spaces are among the largest regions within the myoplasm devoid of tubules (Fig. 3D). Similar to the x–z view in the mammalian fibres, loops of t-tubules outline the myofibrils. The densities of tubules at a given distance from the edge of each nucleus (regions of PI labelling) were measured using a 3D Euclidean distance map of the cytoplasmic space. In plots of the densities of the tubules as a function of distance to the edge of the PI stained nuclei in rat and toad fibres, an increase in the tubular density was observed between 250 and 450 nm (Fig. 3E and Fig. 3F, respectively). PI stains DNA, not the entire nucleus (LePecq and Paoletti, 1967), and so probably underestimates the true boundary of this organelle (i.e. nuclear envelope). The distance between the tubules and the nuclear envelope can therefore be assumed to be shorter, which probably form a junction (Peachey, 1965). The dense packing of tubules at the nuclear envelope is a result of several myofibrils encasing the nucleus. The dense cage of tubules could either fully

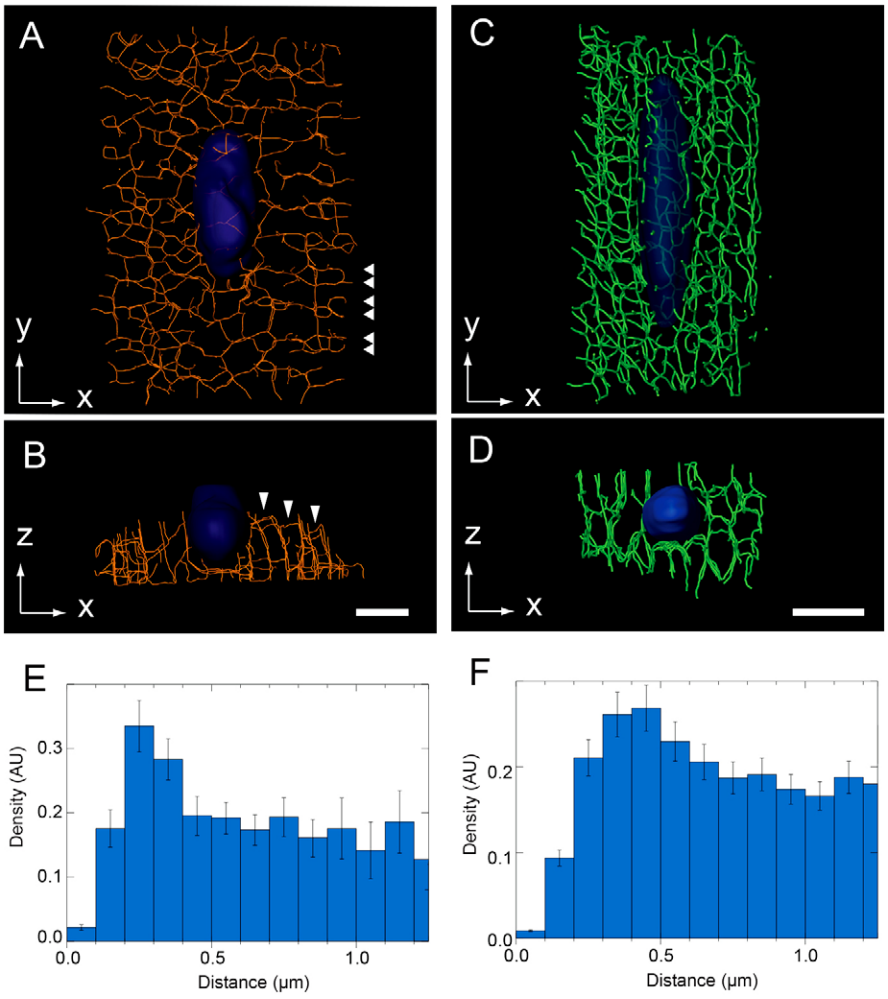

Fig. 3. Spatial relationship between the t-system and nuclei of mammalian and amphibian skeletal muscle. (**A**) The longitudinal lateral view of a peripherally located nucleus vitalized with PI (blue) and the skeleton of the t-system (orange) in a mechanically skinned rat EDL fibre. (**B**) The orthogonal (transverse view) of a 5-µm-deep volume illustrates that the nucleus is closely surrounded by tubules that extend deeper into the fibre. Arrowheads indicate previously reported sub-sarcolemmal tubules that extend near the periphery of the fibre. (**C**) The longitudinal view of a centrally located nucleus (blue) and the skeleton of the t-system (green) in the toad illustrates the dense tubular mesh wrapping around the nuclei. (**D**) The orthogonal (transverse) view of a 5-µm-deep volume of the skeleton highlights the cytoplasmic space devoid of tubules, occupied by the nucleus. (**E,F**) Analysis of the density of tubules as a function of the Euclidean distance from the edge of the region of PI labelling in rat (E) and toad (F) fibres indicate a near-uniform density of tubules in cytoplasmic regions further than ~0.75 µm away. In both species, an ~25–50% increase in the tubule densities was observed between 0.2 and 0.7 µm from the edge of the PI staining. Scale bars: 5 µm.

circumscribe the nucleus, as in toad fibre preparations (Fig. 3D), or form a partial 'basket' that lines the medial face of the nucleus, as in the rat fibre preparations (Fig. 3B).

Estimating tubule diameters and reconstructing t-system ultrastructure

The 3D skeletons constructed out of confocal image stacks of Fluo-5N were used for tracing the local intensities within the t-system. Simultaneous imaging of Fluo-5N trapped within the t-system and lipophilic membrane dye di-4-ANEPPS staining the tubule membranes allowed us to establish that the local Fluo-5N fluorescence intensities along the tubular skeleton were a function of the local tubular volume. See supplementary material Fig. S3.

In image volumes analysed, vacuolated tubules were observed at low abundance. Examining the intensity profile across such vacuolated tubules [typically of full width at half maximum (FWHM) >400 nm] allowed us to study the image properties of tubules that were above the diffraction-limited resolution of the microscope (supplementary material Fig. S4). Using the Poisson distribution of noise estimated by examining vacuolated tubules in each data volume and a measured point spread function (PSF) of the microscope, we simulated the confocal image of an in-plane tubule of variable diameter (d), as illustrated by the examples in Fig. 4A. The image intensity along the midline of the tubule appeared to increase steadily with an increase in the tubular d, although when a non-zero angle between the tubule orientation and the image plane was introduced to the simulation (data not shown), tubules with the same d appeared at higher intensities. This observation was consistent with the previous observation that transverse tubules running orthogonally to the image plane appeared brighter in the confocal image (Jayasinghe et al., 2009), resulting from the interaction between the tubule geometry and the asymmetric confocal PSF, which is elongated in the axial dimension (Fig. 4B). The intensity bias towards the orientation was corrected by re-blurring the confocal image volumes to achieve an effectively spherical PSF (Fig. 4C) as proposed by Soeller and Cannell (Soeller and Cannell, 1999). The mean normalized intensity above background along the centre line of the tubule (equivalent to its skeleton) is shown as a function of its diameter d in Fig. 4D. Tubules narrower than 40 nm resulted in no detectable fluorescence above background while those between ~40 and ~1000 nm showed a steep, near-linear increase in intensity following the re-blurring of the data. The shape of this curve, constructed for each data volume therefore was used for estimating the mean tubule width at each point along the t-system skeleton. The mean width values in

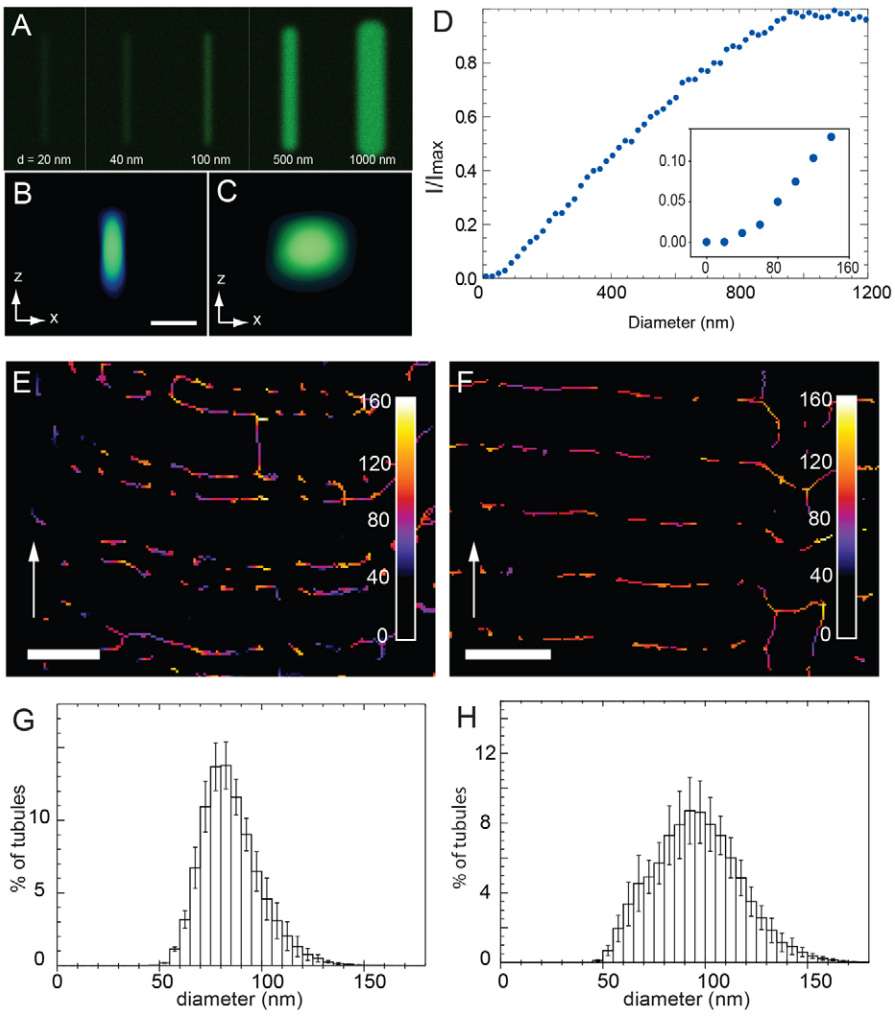

Fig. 4. Simulation of the relationship between t-tubule diameter and the convolved image, and estimation of local tubule diameters of the t-systems in living skeletal muscle fibres. (**A**) A series of simulated images of t-tubules of varying diameters (d). (**B,C**) The point spread function of the imaging system is elongated in the z-dimension compared to x- and y-dimensions, which accentuates the intensity of tubules whose orientations have a non-zero vertical component (B). This is overcome by convolving the 3D confocal data volumes to effectively achieve an approximate symmetry in x-, y- and z-dimensions (C). Scale bar for B and C: 0.5 µm. (**D**) A plot showing the normalized mean intensity above background measured along the centre line of the t-tubule of the confocal fluorescence image following the re-blurring (circles). Note that the narrowest detectable t-tubule corresponds to a diameter of ~40 nm as shown in the magnified region of the plot (inset). (**E,F**) maximum-intensity projections (2-µm-deep) of 3D t-system skeletons of a rat EDL fibre (E) and a toad iliofibularis fibre (F), colour-coded for the estimated mean local tubular diameters. (**G,H**) Histograms showing the percentage of tubules as a function of the mean local diameter in rat (G) and toad (H) fibres. The range and mean diameters are similar (rat and toad fibres were 85.4±14.4 nm and 91.2±20.1 nm, respectively; means ± s.d.). Scale bars for E and F: 2 µm.

regions of the skeleton containing joints, sharp bends or blind ends were corrected to remove the dependence of the intensity on the local tubule geometry as shown previously (Soeller and Cannell, 1999). See supplementary material Fig. S5 for simulations. Image volumes no deeper than 5 µm were analysed for estimating tubule diameters to minimize the effect of time-dependent bleaching and spherical aberration on the depth-dependent intensity in the confocal z-stacks.

Panels E and F of Fig. 4 illustrate 2D z-projections of the rat and toad t-system skeletons across a 2 µm deep volume, colour-coded for the estimated local diameters of the tubules respectively. In these longitudinal views of the skeletons, tubule diameters were most commonly observed in the range of ~70–120 nm in both rat and toad fibres. In both species, longitudinal tubules (extending parallel to the long axes of the fibres, indicated by the white arrows) reported tubule diameters similar to that of transverse tubules. Fig. 4G,H are histograms illustrating the percentage of tubules as a function of the estimated mean local tubule diameters in rat and toad fibres, respectively. The tubule diameters followed an approximately Gaussian distribution in both species, with similar mean tubule diameters for rat and toad muscle (85.4±4.9 nm and 91.2±8.9 nm respectively). However, ~30% of toad t-tubules were found with diameters larger than 100 nm. This was a larger fraction than that observed in rat fibres (~15%).

Effect of cytoplasmic osmolarity on tubular diameters

Previous work has shown that the sealed t-system can change volume in response to changes in osmolarity with minimal change to dye concentration in the optical slice or tubular Ca^{2+} for osmolalities >200 mosmol/kg (Launikonis and Stephenson, 2004). The influx or efflux of water to or from the t-system of skinned fibres also results in a proportional change in ionic strength within this sealed compartment, which exponentially affects the fluorescence intensity of Fluo-5N trapped within the t-system (see supplementary material Fig. S7) (Launikonis and Stephenson, 2004). The fluorescence intensity of tubules observed in confocal z-stacks was adjusted to correct for its non-linear dependence on the ionic strength. This provided a useful assay for examining the variation in tubule diameters in response to osmotic stress.

The histogram in Fig. 5A (left) shows the percentage of tubules as a function of the estimated diameters of tubules in rat fibres incubated in iso-osmotic internal solution (280 mosmol/kg). A near-Gaussian distribution with a mean of ~86 nm was observed in the estimated tubule diameters. The cytoplasmic volume fraction occupied by the t-system (calculated using the local tubule diameters and lengths) was estimated to be ~0.89% with a mean length of ~182 nm tubules detected per 1 fl of cytoplasm. Little detectable change in the mean tubule diameter of rat fibres was observed between 1000 mosmol/kg (hyper-osmotic) and 200 mosmol/kg (hypo-osmotic) internal solutions

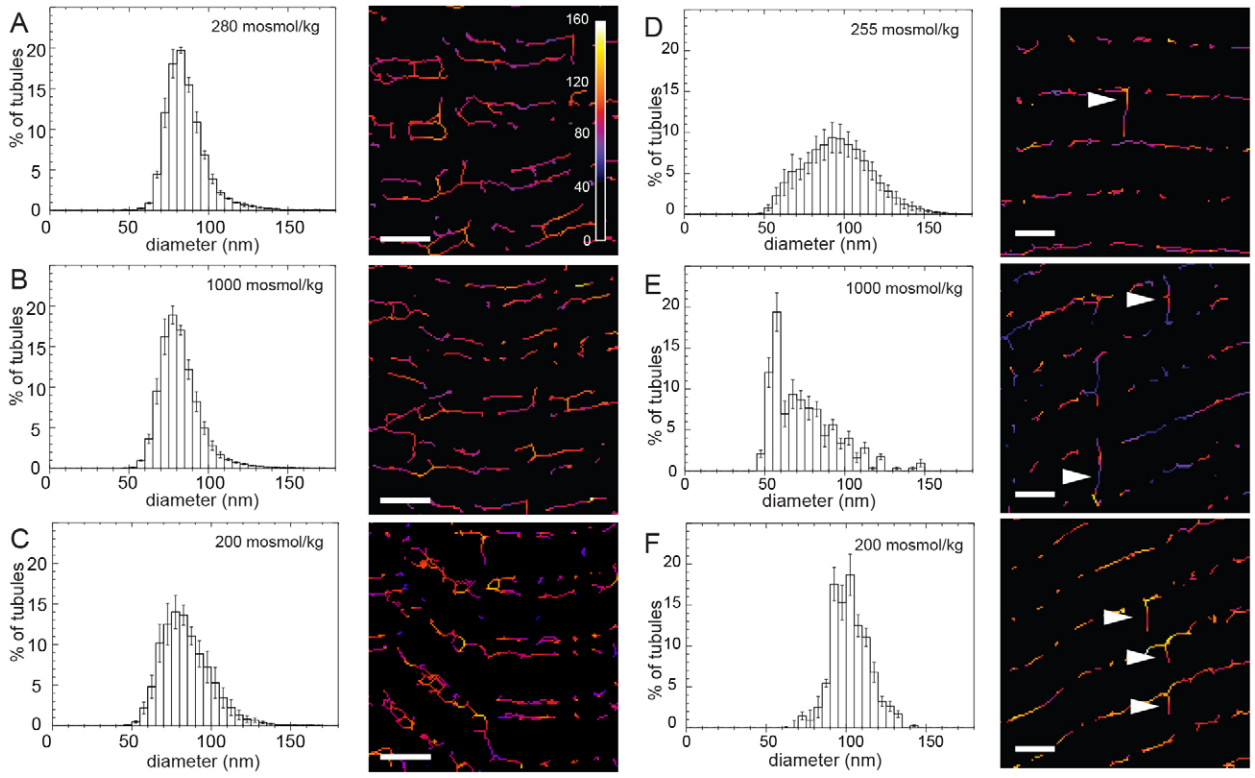

Fig. 5. The effect of osmolarity on the tubule diameters in the rat and toad t-system. (**A–C**) Histograms showing the distributions of estimated mean tubule diameter of mechanically skinned rat EDL fibres that were incubated in (A) isosmotic (280 mosmol/kg); (B) hypo-osmotic (200 mosmol/kg); (C) hyperosmotic (1000 mosmol/kg) internal solutions are shown on the left. 2-µm-deep projections of the colour-coded maps of the local tubule diameters in the respective osmolarity conditions are shown on the right. (**D–F**) Histograms for the estimated mean tubule diameter in skinned toad fibres incubated in (D) isotonic 255 mosmol/kg, (E) hypotonic 200 mosmol/kg and (F) hypertonic 1000 mosmol/kg internal solutions for 15 minutes. The colour-coded maps of the local tubule diameters in isotonic, hypertonic and hypertonic conditions, shown on the right, illustrate that changes in local diameter in the transverse tubules were typically larger than those in the longitudinal tubules (arrowheads). Scale bars: 2 µm. Colour scale illustrates estimated mean tubule widths in nm.

tested (Fig. 5B,C, left). Therefore, the fractional cytoplasmic volumes (~0.92% and ~0.95%, respectively) and mean density (tubule lengths of ~140 nm and ~164 nm per 1 fl of cytoplasm, respectively) remained unaltered. This was reflected in the lack of observable shift in colour in the colour-coded maps of the mean tubule widths (Fig. 5A–C, right). See Table 1 for summary of measurements in different osmotic conditions.

As above, the distribution of tubule widths in toad fibres followed a similar mean (~91 nm and σ=20.1 nm), shown in Fig. 5D (left). Tubules detected at a density of 420 nm per 1 fl of cytoplasm occupied ~1.67% of the fibre volume. When fibres were transferred to a hyper-osmotic internal solution (1000 mosmol/kg), a clear left-shift and a positive-skewing in the distribution of tubule diameters were observed (Fig. 5E, left). The mean tubule diameter in this hyper-osmotic solution dropped by ~13% (to 79.6 nm) while the standard deviation remained unchanged (19.9 nm). However, the detected density of tubules also dropped to ~309 nm per per 1 fl of cytoplasm, suggesting that ~26% of the tubules that were detectable in the isosmotic conditions had shrunk below the size threshold for detection simulated in Fig. 4D. Conversely, an ~7% dilatation of the mean tubule diameter (to 97.5 nm) resulted from bathing the fibre in a hypo-osmotic internal solution (200 mosmol/kg). This was accompanied by a broadening of the percentage distribution of diameters (Fig. 5F, left), indicated by an ~15% increase in σ. This expansion of mean tubule diameter corresponded to an ~40% increase in the volume occupied by the t-system in the cytoplasm (up to ~2.29%). However, the detected tubule density increased only by ~13% (to ~478 nm per per 1 fl of cytoplasm). In reference to the colour-coded 2D map reporting estimated local tubule diameters in iso-osmotic conditions (Fig. 5D, right), a clear drop in the local diameters in hyper-osmotic conditions (Fig. 5E, right) was observed. Notably, regions of longitudinal tubules appeared to retain their diameters (arrowheads). Dilatation in some of the transverse tubules beyond widths of 120 nm under hypo-osmotic conditions was observed while the diameters of longitudinal tubules remained largely unaltered (Fig. 5F, right).

Reconstructing the geometrically realistic t-system

The skeletonization of the 3D confocal data has allowed us to reconstruct and visualize the connectivity of the overall t-system in rat and toad fibres (Figs 1, 2). However, in the experiments and analysis of estimating local tubule widths, a considerable variation in the local region was observed. These measurements were therefore useful for reconstructing the realistic micro-architecture of the t-system by dilating each voxel of the skeleton with a structuring element (SE). Two approaches of rendering tubule image volumes are illustrated in Fig. 6. In the first approach, a symmetric SE was used to dilate the skeleton to a diameter equal to the estimated mean tubule width d (Fig. 6A). Fig. 6B,C illustrate tilted views of the t-systems reconstructed from rat and toad fibres respectively using this approach. These reconstructions yielded both transverse and longitudinal tubules with circular cross-sectional profiles. The transverse tubular networks near the z-lines were observed with great resemblance to the polygonal shapes of t-tubule loops described previously in rat sternomastoid muscle (Franzini-Armstrong and Peachey, 1982). A second rendering approach was used to achieve a more realistic morphology where all transverse tubules were flattened at an aspect ratio of 3.5, assuming that most transverse tubules were found in triads (Franzini-Armstrong et al., 1999) resembling the morphology of a flattened cylinder. This was achieved by using a SE that dilated the t-system skeleton up to a longitudinal width of $0.44\times d$ and transverse width of $1.54\times d$. Tilted views of the t-system reconstructions from rat and toad images are shown in Fig. 5E,F respectively.

Discussion

We have adapted a fluorescence imaging and image analysis protocol previously used for cardiomyocytes (Soeller and Cannell, 1999) for reconstructing the skeletal muscle t-system. However, by trapping dye within the t-system of mechanically skinned fibres, instead of maintaining intact fibres in a physiological solution containing a fluorescence indicator (Soeller and Cannell, 1999; Launikonis and Stephenson, 2002b) we have been able to eliminate residual bath fluorescence and obtain greater contrast (hence, greater sensitivity) in detecting tubules that are typically ~3 times narrower than in cardiac muscle. The combination of these techniques has allowed us to reconstruct the vertebrate t-system in 3D and also quantitatively determine tubular dimensions for the first time. Furthermore, our large volume reconstructions allow the association between the t-system and the nucleus to be described in greater detail than previous imaging studies.

3D ultrastructure of the tubular network

Large areas within the fibres reconstructed here have enabled us to view the t-system network in 3D. The majority of tubules were transverse tubules that wrapped around myofibrils and a smaller fraction of tubules were observed to be extending longitudinally, parallel to the myofibrils. The loops of transverse tubules in the reconstructions were not circular (Fig. 3) and closely resemble

Table 1. Tubular properties under varying osmolarities in rat and toad skinned fibres estimated from rendered confocal volumes

		Osmolarities					
		200 mosmol/kg	255 mosmol/kg	280 mosmol/kg	1000 mosmol/kg	*n* (fibres)	*N* (animals)
Estimated tubular diameters (nm)	Rat	86.3±6.0	–	85.9±6.6	82.2±5.7	6	2
	Toad	97.5±7.4*	91.2±8.2*	–	72.6±8.0*	6	3
Estimated percentage of fibre volume occupied by tubules	Rat	0.95±0.09	–	0.89±0.09	0.92±0.14	6	2
	Toad	2.29±0.11**	1.67±0.10**	–	0.69±0.09**	6	3
Estimated densities of detected tubules (nm/fl)	Rat	164±21	–	182±34	140±42	6	2
	Toad	309±30	420±54 ***	–	309±14	6	3

All values are means ± s.e.m. Asterisks indicate statistical significance at $P<0.05$ for each measurement: *, ** and ***, respectively and d.f.=15.

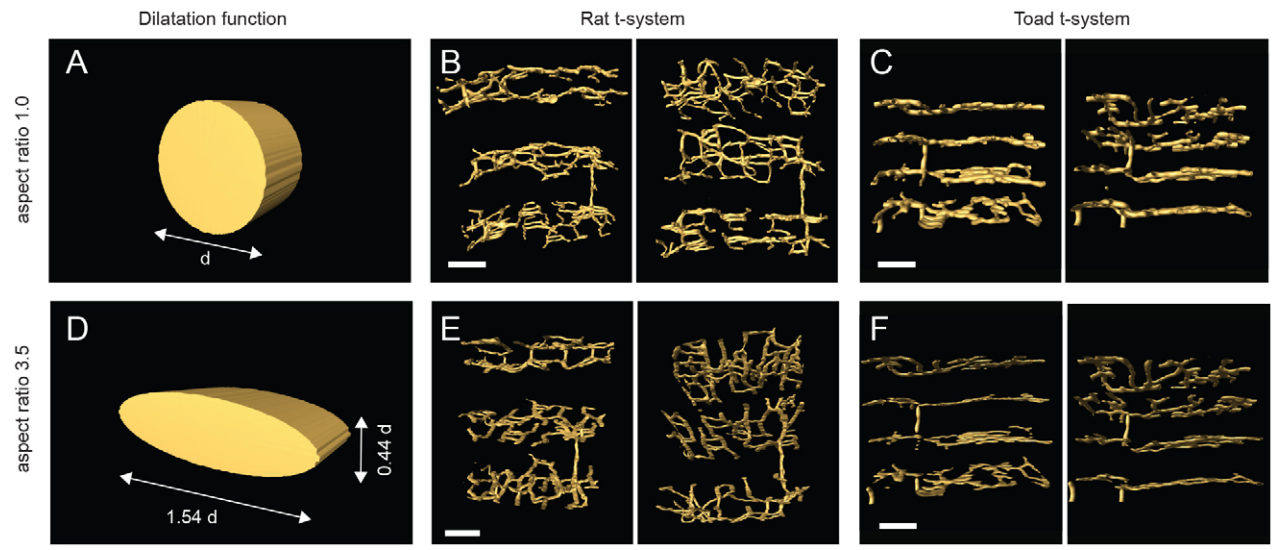

Fig. 6. Visualization of geometrically realistic reconstructions of the rat and toad skeletal muscle t-systems. (**A**) Reconstructions used a structuring element that dilated the local skeleton symmetrically (aspect ratio of 1.0) by a width equal to the estimated mean tubule width (*d*) as shown. (**B**,**C**) Pairs of tilted views of the reconstructions in rat EDL fibres and toad iliofibularis fibres, respectively. (**D**) A more realistic morphology was achieved by dilating the skeleton of transverse tubules asymmetrically (at 1.54*d* in the transverse plane and 0.44*d* longitudinally) to achieve an aspect ratio of 3.5. (**E**,**F**) Tilted views of the rat and toad t-systems rendered assuming that all of the transverse tubules were maintained in a flattened morphology with an average cross-sectional aspect ratio of 3.5. Scale bars: 2 µm.

the 'polygonal' shapes observed in transverse views of skeletal muscle fibres obtained through Golgi stained thick-section EM (Franzini-Armstrong and Peachey, 1981; Franzini-Armstrong and Peachey, 1982). Directionality analyses of the reconstructed t-system indicated that mammalian skeletal muscle contained approximately twice the fraction of longitudinal tubules (~5%) compared to amphibian skeletal muscle fibres (2.2%). However if we apply a factor of 2 against the number of longitudinal tubules in rat and toad muscle to account for the difference in transverse tubule density per sarcomere (which defines the number of longitudinal tubules), then the proportion of longitudinal tubules will be about the same.

The directionality analysis revealed a broad peak in the tubule angle at 0° (transverse plane) in both species analysed. This is a likely result of the shallow angles of the sarcomeric alignment that result in vernier formation (Huxley and Taylor, 1958) or helicoid organization of transverse tubules (Peachey and Eisenberg, 1978). These pseudo-oblique tubules [identified previously as z-tubules (Edwards and Launikonis, 2008)] still remain anchored to the z-line (toad) or the A–I junctions, as apparent in the 3D examination of the skeletons.

Longitudinal tubule morphology revealed by 3D reconstruction also showed features not previously resolved. Longitudinal tubules could be blind ended and also showed looping or curving around the long axis of sarcomeres in addition to simple, straight connections between transverse tubules in both taxa (Figs 1, 2). A pattern to the distribution of longitudinal tubules in mammalian fibres was not obvious. However, within the same volumes of amphibian fibres, there were clear areas devoid of longitudinal tubules and contrasting dense areas of longitudinal tubules that appear to run along this axis of the fibre (Figs 1, 2). These dense volumes of longitudinal tubules would make up the helicoidal structures that allows the t-system to link across misregistered sarcomeres (Peachey and Eisenberg, 1978) but as they also appeared across thicker axial sections, it is not possible to suggest sarcomere misregistration was an underlying cause. The ability of longitudinal tubules to swell or vacuolate under conditions such as fatigue probably underlies a physiological role in temporary storage of metabolites (Lännergren et al., 2000; Edwards and Launikonis, 2008).

The nucleus and t-system

A distinct advantage of reconstructing muscle fibre membranes using confocal microscopy is the visualization of the association of membrane-bound compartments in large volumes. Here we show that the t-system surrounds the nucleus at a high density (Fig. 3). This high density of tubules around the nucleus is the result of abutting myofibrils that run parallel to the long axis of the nuclei. The transverse tubules (and sarcoplasmic reticulum, SR) are simply brought into close proximity to the nuclear envelope by the arrangement. In the reconstructions (Fig. 3), the t-system of rat and toad fibres were observed to fully or partially encase the nucleus. Transverse tubules in frog skeletal muscle have been shown to form dyadic junctions with the nuclear envelope, with the nuclear envelope also being described as continuous with the SR (Peachey, 1965). The presence of t-system junctions with SR and nuclear envelope suggest that EC coupling and excitation-transcription coupling are active in this microdomain. We would therefore expect that Ca^{2+} released from SR during EC coupling influences Ca^{2+} levels inside the nuclear envelope and nucleoplasm. A similar membrane architecture in cardiac muscle at this site and its relevance to excitation-transcription coupling has been described (Wu and Bers, 2006; Wu et al., 2006; Escobar et al., 2011).

Measurements of tubule diameters

The large volume reconstructions of the t-system also allowed determination of local tubular diameter, determined pixel by pixel (Fig. 4). The volumetric sensitivity of fluo-5N trapped in the t-system of skinned fibres was confirmed by simultaneous

measurements of a lipophilic dye (see supplementary material Fig. S3). This result also confirmed that the $[Ca^{2+}]_{t\text{-}sys}$ was mostly uniform throughout the lumen of this structure. This new technique of determining tubular diameters offers a resolution in the order of nm and a detection threshold of ~40 nm, which will be applicable to many situations where the fine morphology of the muscle membranes may be changed, such as in training, disease and age.

The distribution of diameters showed a greater range in the amphibian than the mammalian muscle fibres but the average diameters was between 85 and 90 nm (Fig. 4; supplementary material Fig. S6). The amphibian fibres had many more tubules at larger diameters than the mammalian, which will have implications for tubular resistance and rates of action potential propagation within fibres (Hodgkin, 1954). Overall, the average cross-sectional dimensions of junctional and bare transverse tubules reported from thin-section EM (Rapoport et al., 1969; Dulhunty, 1984) are typically 50–60% smaller than the above estimates. A few considerations are noteworthy in connection to this discrepancy. 3D imaging of the t-system has eliminated the need for any assumptions that were required for determining the orientations of tubules and selecting images in thin-section EM analysis (Dulhunty, 1984). Recent super-resolution direct stochastic optical reconstruction microscopy (dSTORM) data with an in-plane resolution of ~30 nm have demonstrated that diameters of transverse tubules in rat EDL fibres fixed with 4% paraformaldehyde are typically 90 nm in the longitudinal dimension (I. D. J. and Christian Soeller, unpublished data; supplementary material Fig. S6). The imaging of freshly mechanically skinned fibres also avoids any shrinkage associated with gluteraldehyde fixation and dehydration that could lead to under-estimating spatial measurements by ~12% (Eisenberg et al., 1974). The larger tubule diameters estimated from the 3D confocal data could arise from micro-branching of tubules near junctions, reported previously in frog and toad muscle (Peachey and Schild, 1968). If branched tubules remain within close proximity of each other, skeletonization of such diffraction-limited data would detect these structures as a single tubule with a large local volume. However, subsequent EM studies of amphibian muscle have not reported this morphology (Eisenberg and Eisenberg 1968; Dulhunty, 1984), suggesting that these branches may not be as abundant as previously thought. It is also noteworthy that some EM measurements of t-tubule widths agree better with our estimates than the above reports. Cullen et al. estimated the transverse (flattened) width of the transverse tubules at the triad to be ~120 nm in rat EDL fibres. This measurement compares well with the flattened width of rat EDL transverse tubules in our experimental data that measure a mean flattened width of ~132 nm (Cullen et al., 1984). This is further clarified by dSTORM images that have a resolution of 30 nm that show transverse tubules with a resolved diameter of about 90 nm (supplementary material Fig. S6). The larger tubule diameters measured here are also unlikely to be the result of tubule swelling due to the osmotic pressure of any accumulating metabolic products within the sealed t-system. This is evident by the lack of further shrinkage when rat skinned fibres were exposed to solutions with greater osmolarities than 1000 mosmol/kg (Launikonis and Stephenson, 2004) and to a slightly larger t-system volume determined from fluorescence measurements in intact fibres from rat (Launikonis and Stephenson, 2002b). No discrepancy was found between our measurements of the toad t-system volume in skinned fibres (Table 1) and that previously determined in intact fibres from toad (Launikonis and Stephenson, 2002b). The discrepancy in rat may result from our method not detecting all tubules or the combined error of the methods.

An important test of this new technique is to observe tubular diameter changes of rat and toad fibres in response to changes in bathing solution osmolality. The sensitivity of the tubule widths in amphibian skeletal muscle to changes in the osmolality has been documented, as has the relative insensitivity of sealed t-system of rat fibres (Launikonis and Stephenson, 2002b; Launikonis and Stephenson, 2004). We observed a similar response of the rat and toad sealed t-system to changes in bathing solution osmolality using our tubular diameter detection technique as that previously found by averaging all light collected from t-system trapped dye within a confocal plane (Launikonis and Stephenson, 2004).

Consistent with the non-linear response in the t-system volume to changing osmolality, we observed a 7% increase in the tubule diameter in toad fibres when osmolality was reduced by a mere 20% while only a 13% reduction in diameter was seen at an osmolality ~300% above normal. Launikonis and Stephenson (Launikonis and Stephenson, 2002b) observed a 30% increase in the toad t-system volume in response to a 50% reduction in osmolarity, which would correspond to a ~14% increase in the mean tubule diameter, assuming there were no changes in tubular length. Therefore, our measurements of tubule widths are well within the expected range of tubule expansion. It is noteworthy that the distribution of the tubule diameters in toad fibres loses its bell-shape in the hypertonic conditions, suggesting that some tubules may shrink beyond detection in confocal data. Therefore, it is likely that the mean diameter of tubules under osmolalities approaching 1000 mosmol/kg has been over-estimated in these experiments. EM analyses of the transverse tubule morphologies under varying extra-cellular NaCl concentrations have also shown an expansion of the tubule widths along the longitudinal axis (Rapoport et al., 1969) and suggest that the longitudinal sides of the tubular membrane anchoring the junctions are unlikely to be compliant (Rapoport, 1969). Therefore, it is likely that a 7% increase in the mean tubule diameter in a 20% hypotonic solution seen in the above experiments could translate to ~14% expansion in the tubule width in the longitudinal dimension.

Importantly, we are able to spatially resolve changes in tubular diameter (Fig. 4). We have examined the relative changes in the diameters of transverse and longitudinal tubules to osmotic changes and found that the latter was less compliant (Fig. 5). This suggests distinct differences in the transverse and longitudinal tubules (Edwards and Launikonis, 2008). Aquaporin1 has been localized to the transverse tubules (Au et al., 2004), its presence in the longitudinal tubular membranes is yet unclear, making it a candidate. If the membranes of longitudinal tubules are indeed water tight, along with the evidence of restricted diffusion in and out of these tubules (Edwards and Launikonis, 2008), this further consolidates their role as a storage compartment for lactate and other metabolites (Lännergren et al., 2000). However, under hyposmotic conditions, longitudinal tubules would not resist water influxes from neighbouring transverse tubules. The little change in their volume during this process therefore suggests that their membranes are able to withstand greater osmotic colloid

pressures (i.e. less compliant than transverse tubules). Hence, it would be informative to investigate any differences in the scaffolding or structural proteins between longitudinal and transverse tubules. The ability of longitudinal tubules to resist osmolality-dependent volume changes may appear paradoxical given their high propensity to vacuolation (Fraser et al., 1998). Stretch, fatigue, temperature and extracellular concentrations of divalent cations have all been implicated as key factors in the formation of vacuoles (Lännergren et al., 2000; Cooper et al., 2002; Edwards and Launikonis, 2008). Our data suggest that passive expansion due to luminal osmotic colloid pressure is unlikely to be a major contributor for vacuolation.

What does a tubule look like?

While the simultaneous volumetric and membrane imaging experiment confirmed that the assumption of cylindrical geometry of the tubules was reasonable, it is noteworthy that most tubules, in thin-section EM experiments, have appeared as flattened tubes. We must be mindful that neither condition can accurately present to us the physiological condition of the t-system in the living muscle. To estimate what the t-system in a living muscle may look like we have reconstructed all mammalian and toad transverse tubules (Fig. 6) as flattened cylinders based on previous knowledge of the narrow nearest-neighbour edge-to-edge distance (<100 nm) reported previously (Franzini-Armstrong et al., 1999). In connection to this point, the distributions of tubule diameters would more precisely relate to a mean diameter and the actual dimensions of the local tubule would depend on the local aspect ratio. However, previous work has shown that the cross-sectional aspect ratios of transverse tubules are highly sensitive to osmolarity and the extracellular [NaCl] (Rapoport, 1969; Rapoport et al., 1969). This could explain the high variability of the observed aspect-ratios between independent EM studies (Rapoport, 1969; Franzini-Armstrong et al., 1975; Dulhunty et al., 1984) and would warrant a super-resolution imaging approach in studying the triadic transverse tubules under controlled osmotic conditions. The cross-sectional aspect ratios of longitudinal tubules remain poorly documented and there are no reported association of these tubules with junctions. Therefore, these tubules were reconstructed with circular cross-sectional shapes, scaled to the estimated local diameters.

Here we have reconstructed large volumes of the t-system of vertebrate skeletal muscle fibres for the first time. By trapping extracellularly applied fluorescence indicators in the t-system of skinned fibres a highly contrasted image of the t-system can be obtained in a functional fibre. Our imaging has shown previously unresolved details of t-system structure and allowed us to quantify its orientation and diameter. Furthermore, large volume reconstruction has also allowed the association of the t-system within the nucleus to be observed. This technique can also be used for similar imaging with other intracellular organelles such as mitochondria.

Methods

Sample preparation

All experiments were conducted at The University of Queensland. Cane toads (*Bufo marinus*) were obtained from Shawn, Khim and Michael Denson (Brisbane, Qld, Australia) or from Peter Krauss (Mareebra, Qld, Australia). Toads were stunned with a blow to the head and then double pithed in accordance with the procedures approved by the Animal Ethics Committee at the University of Queensland. The iliofibularis muscles were dissected, blotted on filter paper (Whatman No. 1) and pinned out under paraffin oil (Sigma-Aldrich, MO) in a Petri dish lined by a base of Sylgard 184 (Dow Chemicals, MI). For studying mammalian muscle fibres, male Wistar rats (250–300 g) were euthanized by CO_2 asphyxiation under approved procedures and the extensor digitorum longus (EDL) muscles were dissected and pinned out under paraffin oil as above. Small bundles of fibres were dissociated from the muscle and exposed to Na^+-based physiological solution containing 5 mM of membrane-impermeable Fluo-5N pentapotassium salt (Molecular Probes, Life Sciences). As described elsewhere (Launikonis and Stephenson, 2004), individual fibres were separated and mechanically skinned, trapping the dye within the t-system, and mounted onto a chamber built on a No. 1.5 glass coverslip. The fibre was immersed in a standard internal solution containing 100 nM free Ca^{2+} at room temperature (~21℃) and clamped at a sarcomere length of ~2 μm.

Materials and solutions

The dye-containing physiological solution was composed of (mM): NaCl, 112; KCl, 3.3; $CaCl_2$, 2.5; $MgCl_2$, 1, fluo-5N salt, 5; Hepes, 20 (pH adjusted to 7.4 with NaOH) for toad or (mM): NaCl, 145; KCl, 3; $CaCl_2$, 2.5; $MgCl_2$, 2; fluo-5N salt, 5; and Hepes, 10 (pH adjusted to 7.4 with NaOH) for rat. The standard internal solution used for imaging the mechanically skinned fibre contained (mM): K^+, 117; Na^+, 30; EGTA, 1; $HDTA^{2-}$ (Fluka, Buchs, Switzerland), 48.5; Ca^{2+}, 0.0001; Mg^{2+}, 1; Hepes, 60; ATP, 8; and creatine phosphate, 10 for toad; and (mM): Na^+, 36; K^+, 126; Mg^{2+}, 1; EGTA, 1; $HDTA^{2-}$, 48.5; total ATP, 8; creatine phosphate, 10; Hepes, 90; Ca^{2+}, 0.0001; and pH 7.1 for rat. The pH of the internal solutions were adjusted to 7.1 using KOH and the osmolality was ~260±10 and 280±10 mOsmol/kg for toad and rat, respectively.

Image acquisition

Samples were imaged using an Olympus FV-1000 confocal microscope with a 60× 1.35 NA oil-immersion objective (Olympus, Tokyo, Japan). The Fluo-5N was excited using a 488 nm Ar-ion laser (Melles Griot) and the emission detected in the 500–530 nm range using the FV-1000 spectral detector and a pinhole of 0.7 Airy units. Serial confocal image stacks of longitudinally oriented fibres were recorded with a z-spacing of 0.25 μm and pixel sampling finer than 90 nm/pixel. Image stacks were saved as series of 16-bit tagged image file format (TIFF) for further processing.

Image processing and analysis

Confocal image stacks were deconvolved using iterative maximum likelihood Richardson–Lucy algorithm [described by Soeller and Cannell (Soeller and Cannell, 1999)] implemented in IDL 8.2 (Exelis Inc., McLean, Virginia). See supplementary material Fig. S1 for details.

Deconvolved image volumes were re-sampled onto 50×50×50 nm voxel grids in 32-bit TIFF format. A binary mask of the t-system was constructed using the non-linear thresholding protocol outlined previously (Jayasinghe et al., 2009). The binary image volumes were used for generating a 3D skeleton in Amira 5.4 (Visage Imaging, Berlin, Germany). 3D surface rendering of image volumes and reconstructed t-tubular skeletons was performed using Open-dx (Opensource). Directionality analysis of the tubular skeleton was performed on randomly selected 5×5×5 μm image volumes using the 'Directionality' plug-in for Fiji (Liu, 1991; Schindelin et al., 2012).

Imaging osmolarity-dependent changes in tubule diameters

Rat and toad fibres were mechanically skinned trapping 5 mM Fluo-5N within the t-system and mounted onto an imaging chamber ensuring they are not stretched beyond a sarcomere length of ~2 μm. The skinned fibres were bathed in a standard internal solution as described above. The osmolarity of the standard (isosmotic) internal solution was adjusted to 280 mosmol/kg or 255 mosmol/kg for rat and toad fibres respectively. A reference confocal z-stack of the Fluo-5N fluorescence was acquired prior to replacing the internal solution with one whose osmolarity had been adjusted to either 200 mosmol/kg (hypo-osmotic) or 1000 mosmol/kg (hyperosmotic) by adding water or sucrose, respectively. Samples were allowed to equilibrate for 15 minutes at room temperature (~21℃) and a confocal z-stack from an adjacent segment of fibre was acquired. Mono-exponential dependence of the normalized fluorescence intensity (F/F_{max}) on osmolarity x (Eqn 1 where $k=0.0057$) derived from *in vitro* calibration of Fluo-5N (see supplementary material Fig. S7) was used to correct the local Fluo-5N intensities prior to estimating the tubule diameters as described above.

$$F/F_{\max} = (1-F_0)e^{-kx} + F_0 \quad (1)$$

Acknowledgements

We thank D. George Stephenson (La Trobe University, Melbourne) for helpful comments on the manuscript and Christian Soeller (University of Auckland, New Zealand) for supplying the

two-dimensional super-resolution images in supplementary material Fig. S6.

Author contributions

I.D.J. and B.S.L. designed the study, interpreted data and wrote the paper. I.D.J collected, processed and analyzed data.

Funding

This work was supported by an Australian Research Council Discovery Project [grant number DP110102849 to B.S.L.].

Supplementary material available online at
http://jcs.biologists.org/lookup/suppl/doi:10.1242/jcs.131565/-/DC1

References

Au, C. G., Cooper, S. T., Lo, H. P., Compton, A. G., Yang, N., Wintour, E. M., North, K. N. and Winlaw, D. S. (2004). Expression of aquaporin 1 in human cardiac and skeletal muscle. *J. Mol. Cell. Cardiol.* **36**, 655-662.

Cooper, S. J., Chawla, S., Fraser, J. A., Skepper, J. N. and Huang, C. L. (2002). Separation of detubulation and vacuolation phenomena in amphibian skeletal muscle. *J. Muscle Res. Cell Motil.* **23**, 327-333.

Cullen, M. J., Hollingworth, S. and Marshall, M. W. (1984). A comparative study of the transverse tubular system of the rat extensor digitorum longus and soleus muscles. *J. Anat.* **138**, 297-308.

Dulhunty, A. F. (1984). Heterogeneity of T-tubule geometry in vertebrate skeletal muscle fibres. *J. Muscle Res. Cell Motil.* **5**, 333-347.

Dulhunty, A., Carter, G. and Hinrichsen, C. (1984). The membrane capacity of mammalian skeletal muscle fibres. *J. Muscle Res. Cell Motil.* **5**, 315-332.

Edwards, J. N. and Launikonis, B. S. (2008). The accessibility and interconnectivity of the tubular system network in toad skeletal muscle. *J. Physiol.* **586**, 5077-5089.

Edwards, J. N., Cully, T. R., Shannon, T. R., Stephenson, D. G. and Launikonis, B. S. (2012). Longitudinal and transversal propagation of excitation along the tubular system of rat fast-twitch muscle fibres studied by high speed confocal microscopy. *J. Physiol.* **590**, 475-492.

Eisenberg, B. and Eisenberg, R. S. (1968). Selective disruption of the sarcotubular system in frog sartorius muscle. A quantitative study with exogenous peroxidase as a marker. *J. Cell Biol.* **39**, 451-467.

Eisenberg, B. R. and Kuda, A. M. (1975). Stereological analysis of mammalian skeletal muscle. II. White vastus muscle of the adult guinea pig. *J. Ultrastruct. Res.* **51**, 176-187.

Eisenberg, B. R. and Kuda, A. M. (1976). Discrimination between fiber populations in mammalian skeletal muscle by using ultrastructural parameters. *J. Ultrastruct. Res.* **54**, 76-88.

Eisenberg, B. R., Kuda, A. M. and Peter, J. B. (1974). Stereological analysis of mammalian skeletal muscle. I. Soleus muscle of the adult guinea pig. *J. Cell Biol.* **60**, 732-754.

Endo, M. (1964). Entry of a Dye into the Sarcotubular System of Muscle. *Nature* **202**, 1115-1116.

Escobar, M., Cardenas, C., Colavita, K., Petrenko, N. B. and Franzini-Armstrong, C. (2011). Structural evidence for perinuclear calcium microdomains in cardiac myocytes. *J. Mol. Cell. Cardiol.* **50**, 451-459.

Franzini-Armstrong, C. and Peachey, L. D. (1981). Striated muscle-contractile and control mechanisms. *J. Cell Biol.* **91**, 166-186.

Franzini-Armstrong, C. and Peachey, L. D. (1982). A modified Golgi black reaction method for light and electron microscopy. *J. Histochem. Cytochem.* **30**, 99-105.

Franzini-Armstrong, C., Landmesser, L. and Pilar, G. (1975). Size and shape of transverse tubule openings in frog twitch muscle fibers. *J. Cell Biol.* **64**, 493-497.

Franzini-Armstrong, C., Ferguson, D. G. and Champ, C. (1988). Discrimination between fast- and slow-twitch fibres of guinea pig skeletal muscle using the relative surface density of junctional transverse tubule membrane. *J. Muscle Res. Cell Motil.* **9**, 403-414.

Franzini-Armstrong, C., Protasi, F. and Ramesh, V. (1999). Shape, size, and distribution of Ca^{2+} release units and couplons in skeletal and cardiac muscles. *Biophys. J.* **77**, 1528-1539.

Fraser, J. A., Skepper, J. N., Hockaday, A. R. and Huang, C. L. (1998). The tubular vacuolation process in amphibian skeletal muscle. *J. Muscle Res. Cell Motil.* **19**, 613-629.

Hodgkin, A. L. (1954). A note on conduction velocity. *J. Physiol.* **125**, 221-224.

Huxley, A. F. and Taylor, R. E. (1958). Local activation of striated muscle fibres. *J. Physiol.* **144**, 426-441.

Jayasinghe, I. D., Cannell, M. B. and Soeller, C. (2009). Organization of ryanodine receptors, transverse tubules, and sodium-calcium exchanger in rat myocytes. *Biophys. J.* **97**, 2664-2673.

Jayasinghe, I. D., Lo, H. P., Morgan, G. P., Baddeley, D., Parton, R. G., Soeller, C. and Launikonis, B. S. (2013). Examination of the subsarcolemmal tubular system of mammalian skeletal muscle fibers. *Biophys. J.* **104**, L19-L21.

Krolenko, S. A. and Lucy, J. A. (2001). Reversible vacuolation of T-tubules in skeletal muscle: mechanisms and implications for cell biology. *Int. Rev. Cytol.* **202**, 243-298.

Krolenko, S. A., Amos, W. B. and Lucy, J. A. (1995). Reversible vacuolation of the transverse tubules of frog skeletal muscle: a confocal fluorescence microscopy study. *J. Muscle Res. Cell Motil.* **16**, 401-411.

Lamb, G. D., Junankar, P. R. and Stephenson, D. G. (1995). Raised intracellular $[Ca^{2+}]$ abolishes excitation-contraction coupling in skeletal muscle fibres of rat and toad. *J. Physiol.* **489**, 349-362.

Lännergren, J., Bruton, J. D. and Westerblad, H. (2000). Vacuole formation in fatigued skeletal muscle fibres from frog and mouse: effects of extracellular lactate. *J. Physiol.* **526**, 597-611.

Launikonis, B. S. and Stephenson, D. G. (2002a). Properties of the vertebrate skeletal muscle tubular system as a sealed compartment. *Cell Biol. Int.* **26**, 921-929.

Launikonis, B. S. and Stephenson, D. G. (2002b). Tubular system volume changes in twitch fibres from toad and rat skeletal muscle assessed by confocal microscopy. *J. Physiol.* **538**, 607-618.

Launikonis, B. S. and Stephenson, D. G. (2004). Osmotic properties of the sealed tubular system of toad and rat skeletal muscle. *J. Gen. Physiol.* **123**, 231-247.

LePecq, J. B. and Paoletti, C. (1967). A fluorescent complex between ethidium bromide and nucleic acids. Physical-chemical characterization. *J. Mol. Biol.* **27**, 87-106.

Liu, Z. Q. (1991). Scale space approach to directional analysis of images. *Appl. Opt.* **30**, 1369-1373.

Melzer, W., Herrmann-Frank, A. and Lüttgau, H. C. (1995). The role of Ca^{2+} ions in excitation-contraction coupling of skeletal muscle fibres. *Biochim. Biophys. Acta* **1241**, 59-116.

Peachey, L. D. (1965). The sarcoplasmic reticulum and transverse tubules of the frog's sartorius. *J. Cell Biol.* **25** Suppl, 209-231.

Peachey, L. D. and Eisenberg, B. R. (1978). Helicoids in the T system and striations of frog skeletal muscle fibers seen by high voltage electron microscopy. *Biophys. J.* **22**, 145-154.

Peachey, L. D. and Schild, R. F. (1968). The distribution of the T-system along the sarcomeres of frog and toad sartorius muscles. *J. Physiol.* **194**, 249-258.

Posterino, G. S., Lamb, G. D. and Stephenson, D. G. (2000). Twitch and tetanic force responses and longitudinal propagation of action potentials in skinned skeletal muscle fibres of the rat. *J. Physiol.* **527**, 131-137.

Rapoport, S. I. (1969). A fixed charge model of the transverse tubular system of frog sartorius. *J. Gen. Physiol.* **54**, 178-187.

Rapoport, S. I., Peachey, L. D. and Goldstein, D. A. (1969). Swelling of the transverse tubular system in frog sartorius. *J. Gen. Physiol.* **54**, 166-177.

Schindelin, J., Arganda-Carreras, I., Frise, E., Kaynig, V., Longair, M., Pietzsch, T., Preibisch, S., Rueden, C., Saalfeld, S., Schmid, B. et al. (2012). Fiji: an open-source platform for biological-image analysis. *Nat. Methods* **9**, 676-682.

Soeller, C. and Cannell, M. B. (1999). Examination of the transverse tubular system in living cardiac rat myocytes by 2-photon microscopy and digital image-processing techniques. *Circ. Res.* **84**, 266-275.

Wagenknecht, T., Hsieh, C. E., Rath, B. K., Fleischer, S. and Marko, M. (2002). Electron tomography of frozen-hydrated isolated triad junctions. *Biophys. J.* **83**, 2491-2501.

Wu, X. and Bers, D. M. (2006). Sarcoplasmic reticulum and nuclear envelope are one highly interconnected Ca^{2+} store throughout cardiac myocyte. *Circ. Res.* **99**, 283-291.

Wu, X., Zhang, T., Bossuyt, J., Li, X., McKinsey, T. A., Dedman, J. R., Olson, E. N., Chen, J., Brown, J. H. and Bers, D. M. (2006). Local InsP3-dependent perinuclear Ca^{2+} signaling in cardiac myocyte excitation-transcription coupling. *J. Clin. Invest.* **116**, 675-682.